

# Design and Comparison of Electrically Excited Double Rotor Flux Switching Motor Drive Systems for Automotive Applications

Xing Zhao, Shuangxia Niu, and Weinong Fu

(Invited)

**Abstract**—This paper presents a cost-effective driving system for automotive applications based on a double rotor electrically excited flux switching machine (FSM). Benefiting from a double rotor topology, this FSM can realize a drum winding design and thus winding ends are effectively shorten and the copper loss is mitigated. The machine structure, operation principle and design consideration are studied and further verified by time-stepping finite element method. Moreover, three topologies of drive circuit for the proposed FSM are introduced. By using electromagnetic-circuit coupling simulation, a comparison between three different three drive systems are performed, with focus on the system cost and overall electromagnetic performance, especially the effect of current control and torque ripple. A prototype is established and tested. Relevant experimental results verify the effectiveness of the proposed new FSM drive system.

**Index Terms**—Double rotor, electrically excited, flux switching machine, low cost applications.

## I. INTRODUCTION

THE principle of flux switching was first proposed in a single-phase flux-switching alternator in 1955 [1]. Later on, permanent magnet (PM) is introduced into the machine design and further various flux switching permanent magnet (FSPM) machine are presented. Due to its high efficiency and power density, FSPM machines have been extensively investigated over the past decades [2]-[5]. Whereas, in concern of the high cost and unstable price of PM materials, researchers tend to find new topologies of flux switching machine (FSM) which use reduced PMs or even no PMs [6]-[11]. Therefore, the hybrid excited and electrically excited FSMs have been increasingly investigated. To further improve the machine performance as well as reduce the control system cost, various kinds of FSM drive topologies and control topologies have been investigated [12]. However, most of them need sophisticated methodology.

By simply replacing PMs with DC field coils, electrically excited FSM is proposed and investigated for the automotive application [13]. It is demonstrated that this proposed FSM

drive system has a comparable power density and efficiency with those of PM brushed motor drive system. However, this electrically excited FSM topology uses overlapping full-pitch coils for both AC armature winding and DC field winding, which inevitably leads to relatively long winding ends. Hence, the copper loss is considerable, and efficiency is reduced.

To shorten the winding ends, non-overlapping short-pitch is a natural choice. With such a winding structure, a segmental rotor structure is designed to realize the mechanism of flux switching in [14]. However, the rotor should be fabricated by pressing rotor segments onto a nonmagnetic shaft. Besides, the positioning is difficult which involves the use of holes in the shaft as well as protuberances in the segments. Therefore, the manufacturing process is relatively complicated and not suitable for mass production. Inspired by the Double rotor toroidally wound PM machine presented in [15], in this paper, a single-phase electrically excited FSM with double rotors is proposed in this paper. Benefiting from Double rotor topology, the proposed machine is more suitable to be designed with a pancake structure and be conveniently applied in automotive cooling applications, by fixing the stator onto a stationary frame and then integrating the outer rotor to the fan blades. This paper is organized as follows. In Section II, the machine configuration, operation principle and some design analysis are discussed. In Section III, control strategy is presented. And three different topologies of drive circuit are analyzed and compared for the proposed FSM in terms of cost and overall electromagnetic performance. In Section IV, some experimental results will be presented to verify the previous theoretical analysis. Finally, conclusions will be drawn in Section V.

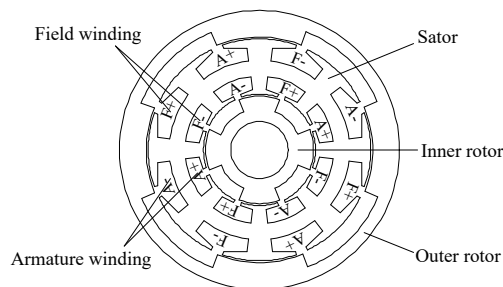


Fig. 1. Configuration of the proposed FSM.

## II. MACHINE STRUCTURE AND OPERATION PRINCIPLE

### A. Machine Structure

Manuscript was submitted for review on 08, May, 2018.

This work was supported by the Research Grant Council of the Hong Kong Government under Project PolyU 152509/16E, 1ZE5P, and in part by the National Natural Science Foundation of China under Grant 51707171.

Xing. Zhao is with the Department of Electrical Engineering, Hong Kong Polytechnic University, Hong Kong (e-mail: xing.hi.zhao@polyu.edu.hk).

Shuangxia. Niu is with the Department of Electrical Engineering, Hong Kong Polytechnic University, Hong Kong (e-mail: eesxniu@polyu.edu.hk).

Weinong. Fu is with the Department of Electrical Engineering, Hong Kong Polytechnic University, Hong Kong (e-mail: eewnfu@polyu.edu.hk).

Digital Object Identifier 10.30941/CESTEMS.2018.00023

The structure of the proposed FSM is presented in Fig.1, which can be regarded as an integration of FSM and double rotor machine. These two rotors share a common stator yoke on which the armature coils and field coils are alternately and toroidally wound, as a result, both coil sides are fully utilized. The advantage of this Double rotor topology is distinct. Firstly, the internal space of the machine is fully utilized, and slot fill factor is improved. Secondly, the flux switching function for both machines can be realized with only one set of armature and field windings, which means the structure is simplified. Thirdly, winding ends are significantly shortened compared to the traditional electrically excited FSMs, correspondingly, the copper loss is reduced, and the overall efficiency is improved. Finally, the outer rotor and inner rotor can be mechanically connected together by an end disc to form an integral cup shaped rotor, which means the torque can be overlapped to boost torque density. Besides, no PM are placed on rotor, thus this machine owns good mechanical strength.

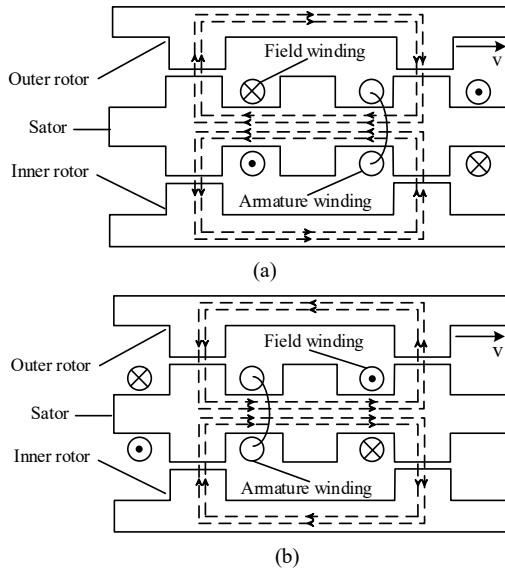


Fig. 2. Flux distribution of the proposed FSM. (a)  $\theta=0^\circ$ . (b)  $\theta=45^\circ$ .

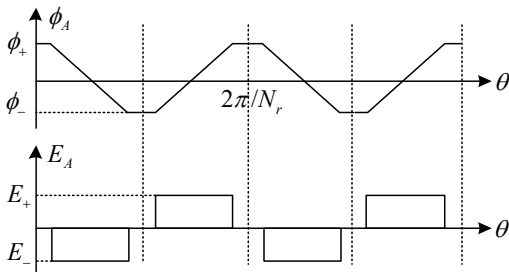


Fig. 3. Schematic coil flux linkage and induced voltage.

### B. Operation Principle

Different with the traditional electrically excited FSMs, the coils of this proposed machine are wound on the stator yoke instead of the stator teeth. To illustrate the operation principle of the proposed machine more clearly, the flux distribution at different rotor positions are presented in Fig. 2. It can be seen that at the rotor angular position  $\theta = 0^\circ$ , rotor poles are aligned with the stator poles, and the flux linkage of armature coils is generated with the left field coils. And when the rotor moves to

the angular position  $\theta = 45^\circ$ , in other words, the rotor poles slip over a polar distance and are aligned with the next stator poles, the flux linkage of armature coils is generated with the right field coils instead of the original left one. And because

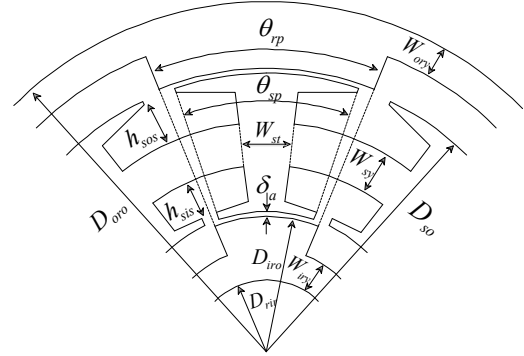


Fig. 4. Some general dimensions of the proposed FSM.

TABLE I  
Dimension Parameters of The Proposed FSM

Symbol	Parameter	Value
$N_s$	Stator pole number	8
$N_r$	Rotor pole number	4
$D_{oro}$	Outer rotor outer diameter	88 mm
$D_{iro}$	Inner rotor outer diameter	34 mm
$D_{ri}$	Inner rotor inner diameter	18 mm
$D_{so}$	Stator outer diameter	70 mm
$L$	Stack length	40 mm
$\delta_a$	Air gap length	0.5 mm
$W_{ory}$	Outer rotor yoke width	4 mm
$W_{oy}$	Inner rotor yoke width	4 mm
$W_{sy}$	Stator yoke width	5 mm
$W_{st}$	Stator tooth width	6 mm
$h_{sos}$	Stator outer slot depth	6 mm
$h_{sis}$	Stator inner slot depth	6.4 mm
$\theta_{rp}$	Rotor pole arc	$43^\circ$
$\theta_{sp}$	Stator pole arc	$38^\circ$

TABLE II  
SPECIFICATIONS OF THE PROPOSED FSM

Parameter	Value
Voltage	12 V
Torque	0.4 Nm
Power	80 W
Field MMF	250 At
Armature MMF	250 At
Turn number per field coil	25
Turn number per armature coil	25
Field wire diameter	1.1 mm
Armature wire diameter	1.1 mm
Electric loading	24 A/mm
Magnetic loading	0.25 T

adjacent two DC field coils have entirely opposite polarities, the armature flux linkage has different directions at different positions accordingly, therefore, the function of flux switching is realized. With bipolar flux linkage excited in armature coils, periodical induced voltage is also generated as shown in Fig. 3. Hence, a steady electromagnetic energy conversion is realized.

### C. Finite Element Analysis

To verify the feasibility of the proposed FSM, time-stepping

finite element approach is used to evaluate its electromagnetic performance, by using a commercial software Ansys Maxwell. Some general dimensions are described in Fig. 4, along with their detail design values listed in Table I. The outer diameter is 88mm, stack length is 40mm, air gap length is 0.5mm, and so on. Further, its rated specifications are listed in Table II.

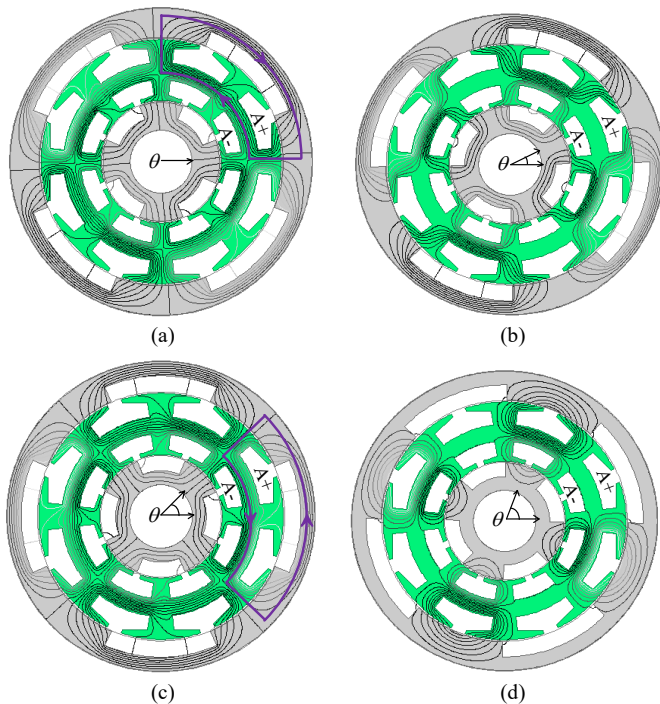


Fig. 5. No-load flux distribution excited by 10A DC field current. (a) Positive maximum armature flux at  $\theta=0^\circ$ . (b) Zero armature flux at  $\theta=22.5^\circ$ . (c) Negative maximum flux at  $\theta=45^\circ$ . (d) Zero armature flux at  $\theta=67.5^\circ$ .

Fig.5 shows the no-load magnetic field distributions of the motor at four different rotor positions with a constant DC field current. It can be seen that when the rotor poles align with the stator poles, as shown in Fig. 5(a) and (c), the flux linkage of the armature coils reaches the maximum magnitude (either positive or negative values), and when the rotor poles align with the stator slots, as shown in Fig. 5(b) and (d), the flux linkage of the armature coils becomes zero as the flux excited by DC field coils will all be short-circuited. Therefore, as the rotor rotates, under the condition of constant DC field current, a bipolar flux linkage will be induced in the armature winding, which is in accordance with the previous theoretical analysis.

At the rated speed 1000 r/min, the no-load flux linkage and induced voltage of the armature winding is further calculated with different field current, as presented in Fig. 6. It can be noticed that the armature flux linkage is bipolar alternating as expected and the induced phase voltage has a good trapezoidal pattern and the its top is relatively broad, which means this machine is more suitable for brushless DC operation.

Moreover, the no-load self-inductance characteristic of the DC field winding and AC armature winding, and their mutual-inductance are calculated and plotted as presented in Fig. 7. It can be seen that the self-inductance of AC armature winding is almost constant, which means this new machine is essentially different from switching reluctance machine, which utilizes the

variation of armature self-inductance to produce reluctance torque. And meanwhile, self-inductance of DC field winding is also relatively steady, which ensures little induced voltage will be induced in the DC field terminal during a constant DC field

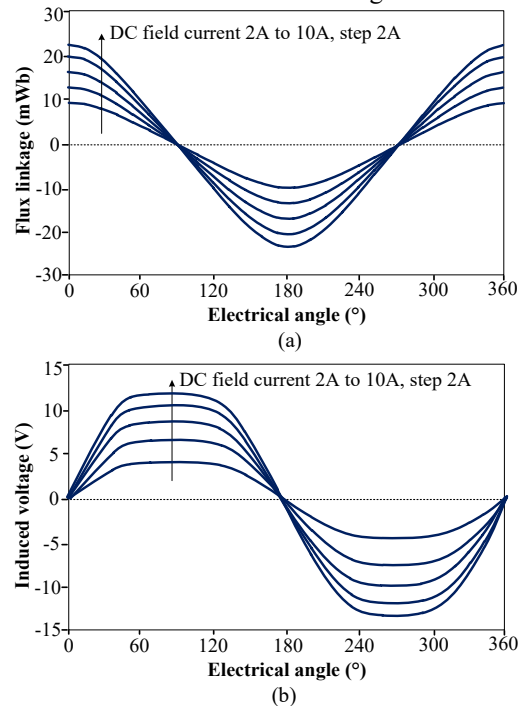


Fig. 6. Electromagnetic performance with different DC field current at 1000 rpm. (a) Phase flux linkage. (b) Induced phase voltage.

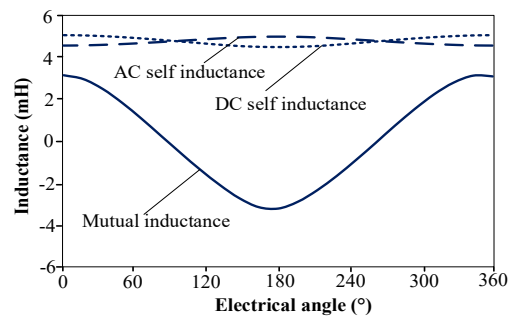


Fig. 7. No-load self-inductance of AC and DC coils, and mutual inductance.

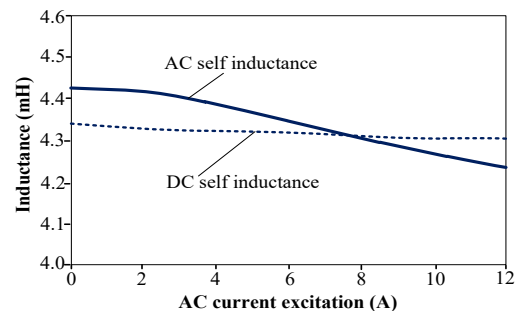


Fig. 8. Self-inductance with different load current, when DC current is 10A.

current injection. The mutual-inductance between the AC armature winding and DC field winding changes periodically with the electrical angle, which is the fundamental principle in the proposed machine to produce effective torque.

The self-inductance greatly influences the effect of current control, including commutation time and ripple performance.

Meanwhile, it's relationship between the current excitation is also needed to be revealed for no-line determination of control parameters. Fig. 8 shows the average value of self-inductance with different AC current excitation, when DC current is 10A. In general, the DC self-inductance is almost constant, while the AC self-inductance decreases when load increases.

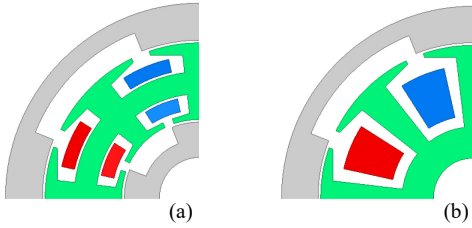


Fig. 9. Finite element models for comparison. (a) Proposed. (b) Existing.

	Proposed FSM	Existing FSM
Same current density	5A/mm <sup>2</sup>	5A/mm <sup>2</sup>
Average torque	0.48Nm	0.58Nm
Same copper loss	20W	20W
Average torque	0.48Nm	0.38Nm

#### D. Comparison with existing single rotor structure.

To verify the effectiveness of this new double rotor design, a comparison is performed between the existing single rotor FSM and the proposed double rotor FSM. Two finite element models are built in this paper, as shown in Fig. 9. They have the same outer diameter, stack length and air gap length. Besides, the slot fill factor and current density are also fixed the same. Table III presents the calculated performance for two models. It can be seen, the proposed double rotor topology can generate higher torque per copper loss, benefiting its reduced winding ends.

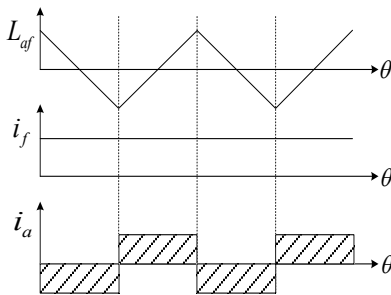


Fig. 10. Current mode of the proposed FSM.

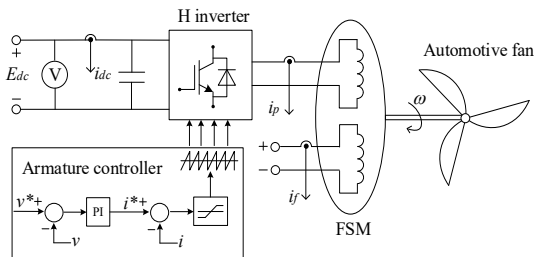


Fig. 11. Drive system and control block based on the proposed FSM.

### III. DRIVE SYSTEM COMPARISON

#### A. Torque Components and Control Strategy

From a magnet-co-energy perspective, the electromagnetic

torque of the proposed FSM can be deduced as:

$$T_e = \frac{1}{2} i_f^2 \frac{dL_f}{d\theta} + \frac{1}{2} i_a^2 \frac{dL_a}{d\theta} + i_f i_a \frac{dL_{af}}{d\theta} \quad (1)$$

where  $L_a$  and  $L_f$  are the self-inductance of AC armature and DC field windings, respectively.  $L_{af}$  is the mutual inductance between these two sets of windings.  $i_a$  and  $i_f$  are the current of AC armature and DC field winding, respectively.  $\theta$  is the rotor angular position. From this equation, it can be seen that the electromagnetic torque of the proposed machine consists of these three components, namely cogging torque due to the variation of field self-inductance, reluctance torque due to the variation of armature self-inductance as well as mutual torque due to the variation of mutual-inductance between these two set of windings. Based on the inductance characteristics shown in Fig. 7, the variation of the self-inductance of armature or field winding is much smaller than that of mutual-inductance, the mutual torque will be dominant, while the cogging torque and reluctance torque can be ignored.

The current control mode for the proposed FSM is given in Fig. 10. The DC field current should be regulated as a maximum constant value to establish a steady and maximum air gap flux density, and in this way, the most efficient rated operation can be achieved regardless of load current. As for the AC armature terminal, the polarity of injected current should in line with the variation of mutual inductance. Specifically, positive armature current should be injected when mutual-inductance increases, and instead negative armature current should be injected when mutual-inductance decreases. Only in this way, a steady multi-inductance torque can be produced. The whole drive system and its control block is further presented in Fig. 11. Dual loop control is used to regulate the speed and current of the system meet the requirement of automotive fan applications.

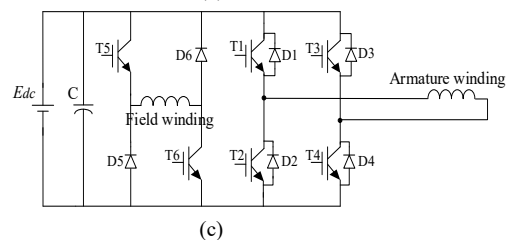
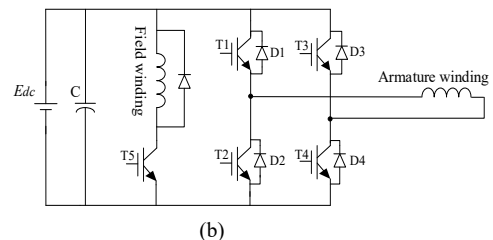
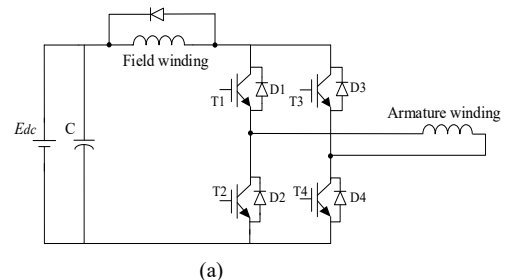


Fig. 12. Three drive circuits for regulating DC field current and AC armature current. (a) Topology I. (b) Topology II. (c) Topology III.

### B. Alternative Three Drive Topologies

This Section focuses the comparison of three different drive topologies for the proposed FSM as shown in Fig.12. In three drive circuits, the AC armature winding is always connected to an H bridge converter to obtain a bipolar drive current, but the connection modes of DC field winding are different. In the first drive circuit as presented in Fig. 12(a), namely topology I, DC field winding is embedded into the DC bus, which means it is in series with the AC armature winding, and accordingly DC field current can be indirectly controlled when regulating AC armature current. Obviously, no extra switching device is needed for DC field current regulation. Meanwhile, a diode is necessary to be connected in parallel with DC field winding, thus providing a pathway for the energy to return back to the power supply. The second drive circuit is shown in Fig. 12(b), namely topology II, in which DC field winding is arranged in parallel with AC armature winding. DC field current can be controlled by an extra switching device and parallel diode. In this topology, the control of field current and armature current is relatively independent. The third drive circuit is presented in Fig. 12(c), namely topology III, in which DC field winding is connected in parallel with AC armature winding and supplied by an asymmetrical half-bridge converter.

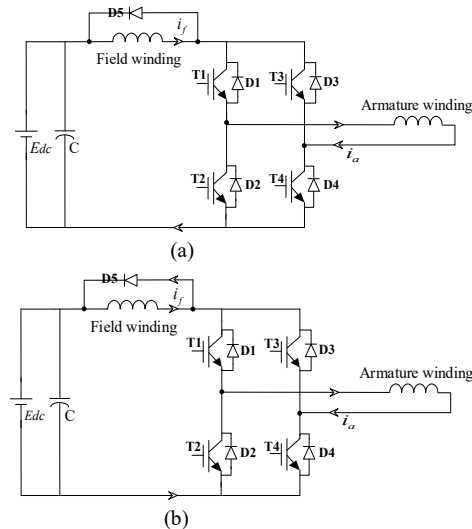


Fig. 13. Current regulation for topology I. (a) T1, T4 on. (b) T1, T4 off.

### C. Transient Analysis for Three Drive Topologies

For topology I, the transient process for the current regulation is presented in Fig. 13. During the steady state operation, when switches T1 and T4 turn on as shown in Fig. 13(a), the current flows out from the positive side of power supply to the DC field winding, passing through the AC armature winding, and finally return to the negative side of power supply. In this process, the power supply transfers its energy to both the field and armature windings in the same loop, and meanwhile, the DC field current and AC armature current synchronously increase to a threshold value. Then, switches T1 and T4 turn off, as shown in Fig. 13(b), at this time, the armature current flows out from the paralleled diodes of the switches T2 and T3, passing through the paralleled

diode of DC field winding to the power supply. During this period, the AC armature winding returns its energy to the power supply with armature current continuously decreasing. Besides, the DC field winding is shorted by the paralleled diode and its magnetic energy is consumed by loop resistance, accordingly, the DC field current decreases along with the armature current. When the armature current decreases until a threshold value, switches T1 and T4 turn on again, and thus the DC field current and AC armature current increase simultaneously again. In that case, DC field current is indirectly but effectively controlled by regulating the magnitude of armature current.

For topology II, its AC armature current and DC field current are independently controlled. The transient process for DC field current regulation is presented in Fig.14. During the steady state operation, when the switch T5 turns on as shown in Fig.14(a), the current flows out from the positive side of the power supply, then passing through the field winding and then return back to the negative side of the power supply. The field current keeps increasing with the power supply transferring its energy to the field winding. When field current increases to a threshold value, the switch T5 turns off. And at that time, the DC field winding is shorted by the parallel diode as shown in Fig.14(b), and the field current keeps decreasing with its energy consumed by the internal resistance. When the DC field current decreases to a threshold value, the switch T5 will turn on again, and thus an effective and independent regulation for the DC field current is achieved during the steady state operation.

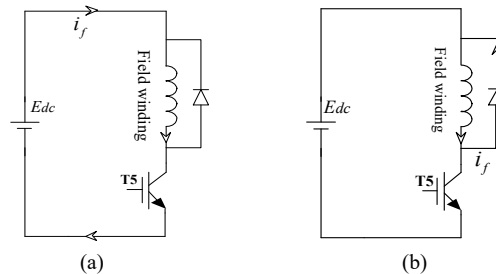


Fig. 14. DC current regulation for topology II. (a) T5 on. (b) T5 off.

For topology III, its control of AC armature current and DC field current is also independent. The transient process for DC field current regulation is further presented in Fig.15. When the switches T5 and T6 turn on as shown in Fig. 15(a), the current flows out from the positive side of power supply, then passing through the DC field winding, and finally return back to the negative side of the power supply. During this period, with the power supply transferring its energy to the DC field winding, DC field current keeps increasing. When it arrives a threshold value, the switches T5 and T6 turn off. At that time, DC field current flows out from two parallel diodes as shown in Fig. 15(b) and keeps decreasing with its energy returning back to power supply. When the field current decreases to a threshold value, the switches T5 and T6 turn on again, and thus an effective and independent current regulation is achieved for the field winding.

### D. Field-Circuit Coupling Simulation

Using field-circuit coupling simulation, the DC field current, AC armature current and output torque, for above three drive topologies are calculated and presented in Fig. 16. For topology

I, as shown in the Fig. 16, the field current can be effectively controlled at a DC 5A, although there is no switching device for

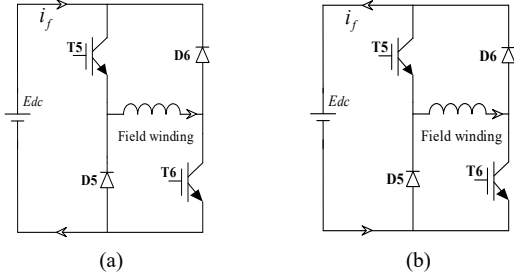


Fig. 15. DC current regulation for topology III. (a) T5, T6 on. (b) T5, T6 off.

field current regulation. The AC armature current can be also controlled as square waveform as expected. A positive average torque can be achieved based on the effective control of DC and AC current excitation. For topology II, as shown in Fig. 17, it can be the current control effect as well as the output torque waveform, are almost the same with that for topology I. It needs to be mentioned, in topology I and topology II, at commutation time when AC current reversal comes, a distinct current spike appears at the DC terminal. As for topology III, as presented in Fig. 18, good current control effect can be achieved with a smooth DC field current and symmetrical AC armature current. The output torque is relatively smooth when compared with that in topology I and II. However, the average torque is reduced, since in topology I and II, the DC current spike bring a toque spike as well, which increases the average torque to some extent. In general, all these three topologies can provide an effective current control and produce positive average torque. However, current spike and torque spike are observed in both topology I and topology II. The main reason for this phenomenon is that the DC filed winding will be shorted by the paralleled diode at the commutation time, as discussed previously in Part B. Some theoretical analysis about this spike will be given as follows.

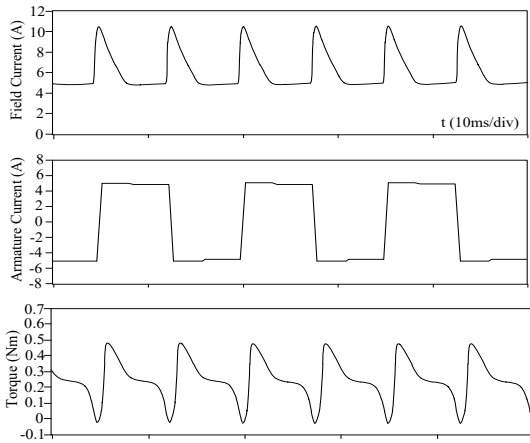


Fig. 16. DC field current, AC armature current and torque. for topology I.

### E. Analysis of Current Spike at Commutation Time

To further explain the reason for the DC field current spike, the electromagnetic relationship in the proposed machine at the commutation time is discussed as follows

The flux linkage of the field winding can be expressed as:

$$\psi_f = L_f \cdot i_f + L_{af} \cdot i_a \quad (2)$$

The induced electromotive voltage of the DC filed winding can be expressed as following:

$$U_f = -\frac{d\psi_f}{dt} \quad (3)$$

Substituting (2) into (3), eq. (4) can be obtained as

$$U_f = -\left(\frac{dL_f}{dt} \cdot i_f + L_f \cdot \frac{di_f}{dt} + \frac{dL_{af}}{dt} \cdot i_a + L_{af} \cdot \frac{di_a}{dt}\right) \quad (4)$$

The  $L_f$  almost remains a constant value with the changing of rotor position, thus eq. (4) can be simplified as

$$U_f = -\left(L_f \cdot \frac{di_f}{dt} + \frac{dL_{af}}{dt} \cdot i_a + L_{af} \cdot \frac{di_a}{dt}\right) \quad (5)$$

At AC armature current reversal time, the DC field winding

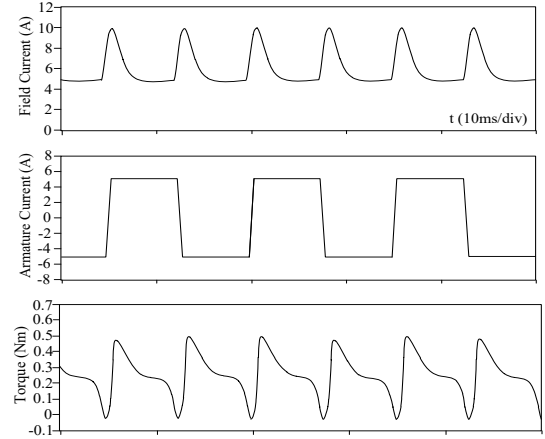


Fig. 17. DC field current, AC armature current and torque. for topology II.

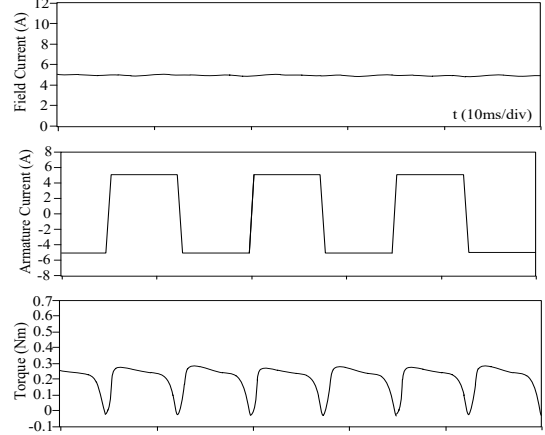


Fig. 18. DC field current, AC armature current and torque. for topology III.

is shorted by the paralleled diode. By ignoring the voltage drop of diode, the loop voltage can be expressed as

$$U_f - R_f i_f = 0 \quad (6)$$

where  $R_f$  is the internal resistance of the DC field winding.

By combining eq. (5) and (6), eq. (7) is derived as

$$e_{af} = -\frac{d(L_{af} \cdot i_a)}{dt} = L_f \cdot \frac{di_f}{dt} + R_f i_f \quad (7)$$

Where  $e_{af}$  is induced voltage excited by the variation of mutual inductance between DC winding and AC winding.

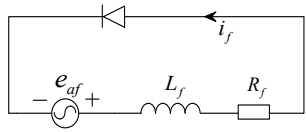


Fig. 19. Equivalent circuit when DC field winding is shorted by parallel diode.

As analyzed in Part A, at the armature current reversal time, mutual-inductance actually begins to decrease. Therefore, when the armature current changes from a positive value to a negative value, a rapid decrease of flux linkage is generated by mutual-inductance and a considerable induced voltage will appear in the DC field winding. As the equivalent circuit shown in Fig.19, due to the existence of mutual induced voltage, the armature winding transfers its magnetic energy to the DC filed winding, thus DC field current will not decrease but instead increases, when shorted by parallel diode at commutation time. Therefore, DC field current spike appears for topology I and topology II.

TABLE IV

COMPARATIVE STUDY WITH DRIVE SYSTEMS BASED ON THE PROPOSED FSM

Number of switching devices	Topology I < Torque II < Torque III
Current scale of parallel diode	Topology I = Torque II > Torque III
Overall inverter cost	Topology I < Torque II < Torque III
Complexity of control strategy	Topology I < Torque II < Torque III
DC current ripple ratio	Topology I = Torque II > Torque III
AC current ripple ratio	Topology I = Torque II = Torque III
Average torque	Topology I = Torque II > Torque III
Torque ripple ratio	Topology I = Torque II > Torque III

F. Comparison of Three Drive Topologies

Based on the above analysis, a comprehensive comparison is presented in the Table IV, from the perspective of inverter cost, control complexity, current control effect and torque capacity. The topology I embedded DC field winding into DC bus, thus no extra switching device is needed for DC current regulation. Therefore, its cost burden is minimized considering switching device as well its drive, are usually the dominant part of inverter cost. Meanwhile, the DC field winding can act as nature passive filter to reduce the current ripple and EMI. It should be pointed out, although a current spike will appear at the DC field terminal in topology I and II, which will inevitably increase the current scale of parallel diode. However, the cost of parallel diode is much lower than the switching device. Therefore, in general, from the perspective of inverter cost burden, topology I is the best choice, then is topology II and finally topology III. Further, when considering the complexity of control strategy, topology I is also the simplest, then is topology II and finally topology III. When the performance of current control and output torque are evaluated, the DC current ripple as well as torque ripple ratio of topology I and II, are much larger than topology III. However, the average torque of topology I and II, is also higher than that of topology III, benefiting from an enhanced DC exciting field at each commutation time. Therefore, in general, the topology I is preferred to drive the proposed FSM, which has the minimum cost burden, simplest control strategy and higher output torque ability. However, it should be pointed the control of topology I is not so flexible due to series feature

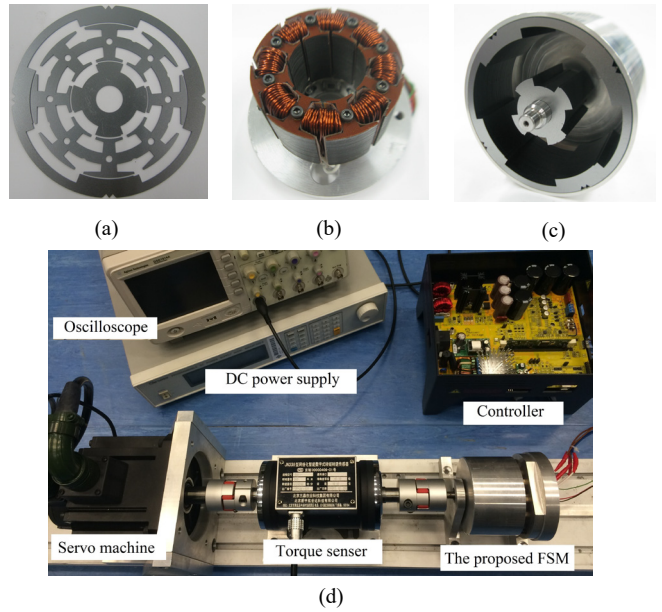


Fig. 20. Machine prototype and experiment platform. (a) Steel laminations. (b) Stator component. (c) Rotor component. (d) Experiment platform.

IV. EXPERIMENTAL VERIFICATION

To demonstrate the feasibility of the proposed double rotor electrically excited FSM system for automotive applications, a prototype has been manufactured. Its steel laminations, stator component and rotor component, are shown in Fig. 20 (a) and (b) and (c), respectively. It should be pointed out that, in order to mount the middle stator onto a disc, some holes are purposely drilled in the stator tooth to set screws. An experiment platform is further established in the laboratory which mainly includes a TI controller to drive the FSM, a servo motor, DC power supply and so on, as presented in Fig. 20(d).

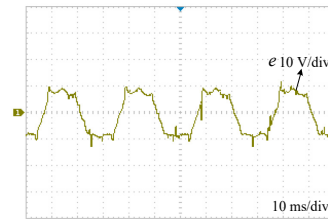


Fig. 21. Measured no-load back EMF at 1000rpm.

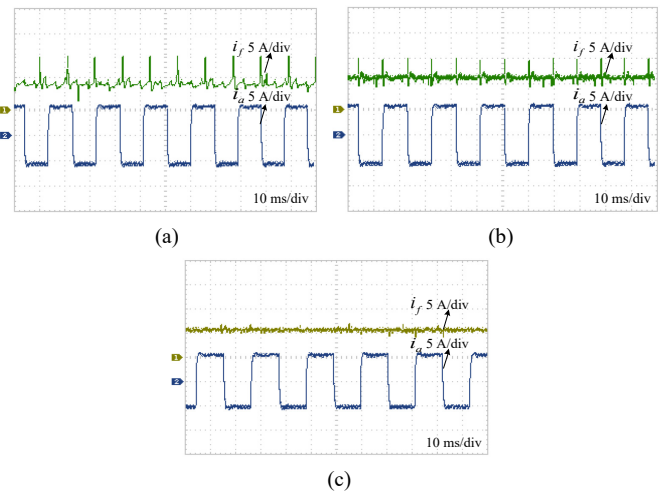


Fig. 22. Measured DC field current and AC armature current after closed-loop control. (a) Topology I. (b) Topology II. (c) Topology III.

The armature no-load back EMF at the rated speed 1000 rpm is measured and shown in Fig.21, which has a good trapezoidal pattern and agrees well with the simulated results. Further, the measured DC field and AC armature current with three different drive topologies are shown in Fig. 22(a), (b), (c), respectively.

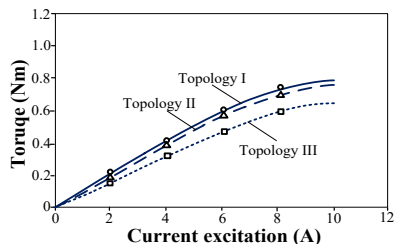


Fig. 23. Torque ability. (a) Topology I. (b) Topology II. (c) Topology III.

It can be seen that the armature current all has a periodic square wave pattern as expected under these three topologies. However, with the topology I and II adopted, there is a periodic currentspike appearing at each commutation time when the armature reversal comes, which agrees with prediction in the previous section. When the topology III is used, much smoother DC field current can be obtained compared with the other two topologies. The torque capacity is also evaluated with different AC current excitation as shown in Fig. 23, in which topology I presents the highest torque. In general, topology I with DC field winding integrated in DC bus, is recommended.

## V. CONCLUSION

A double rotor electrically excited FSM-based drive system is presented in this paper for the automotive fan applications. By creatively integrating an outer rotor and inner rotor FSM, the proposed machine realizes the function of flux switching with a drum winding design. The winding ends are shortened. Therefore, the cost is reduced, and copper loss is mitigated. The machine structure, operation principle and design details are investigated and further verified by FEM. Then, based on the electromagnetic-circuit coupling analysis and prototype testing, three different drive topologies in which the DC field winding is arranged in different ways, are evaluated in terms of system cost, current control effect, as well as torque performance. It is revealed three topologies can all work effectively. When DC field winding is arranged in the DC bus, the converter cost is minimized, however, the current control is not so flexible, and a current spike will emerge at each commutation time. When DC field winding is supplied by an independent inverter, the current control is most flexible and smoother torque waveform can be achieved, although its cost burden is relatively large. The conclusion in this paper can also provide a design guideline for other electrically excited machine-based drive system.

## REFERENCES

- [1] S. E. Rauch and L. J. Johnson, "Design principles of the flux-switch alternators," *Amer. Inst. Elect. Eng. Trans.*, vol. 74III, pp. 1261–1268, 1955.
- [2] Z. Q. Zhu and J. T. Chen, "Advanced flux-switching permanent magnet

brushless machines," *IEEE Trans. Magn.*, vol. 46, no. 6, pp. 1447–1453, Jun. 2010.

- [3] J. T. Chen, Z. Q. Zhu, S. Iwasaki, and R. P. Deodhar, "A novel E-core switched-flux PM brushless AC machine," *IEEE Trans. Ind. Appl.*, vol. 47, no. 3, pp. 1273–1282, May/Jun. 2011.
- [4] R. Cao, C. Mi, and M. Cheng, "Quantitative comparison of flux-switching permanent-magnet motors with interior permanent magnet motor for EV, HEV and PHEV applications," *IEEE Trans. Magn.*, vol. 48, no. 8, pp. 2374–2384, Aug. 2012.
- [5] A. S. Thomas, Z. Q. Zhu, and G. W. Jewell, "Comparison of flux switching and surface mounted permanent magnet generators for high-speed applications," *IET Elect. Syst. Trans.*, vol. 1, no. 3, pp. 111–116, Sep. 2011.
- [6] C. Yu, S. Niu, S. L. Ho, and W. N. Fu, "Design and analysis of a magnetless double rotor flux switching motor for low cost application," *IEEE Trans. Magn.*, vol. 50, no. 11, art. no. 8105104, Nov. 2014.
- [7] Z. Q. Zhu, Z. Z. Wu, D. J. Evans, and W. Q. Chu, "A wound field switched flux machine with field and armature windings separately wound in double stators," *IEEE Trans. Energy Convers.*, vol. 30, no. 2, pp. 772–783, Jun. 2015.
- [8] X. Zhao and S. Niu, "Design of a novel consequent-pole transverse-flux machine with improved permanent magnet utilization," *IEEE Trans. Magn.*, vol. 53, no. 11, pp. 1–5, Nov. 2017.
- [9] X. Zhao and S. Niu, "Design of a novel parallel-hybrid-excited Vernier reluctance machine with improved utilization of redundant winding harmonics," *IEEE Trans. Ind. Electron.*, vol. no. pp. 2018.
- [10] X. Zhao and S. Niu, "Design and optimization of a new magnetic-g geared pole-changing hybrid excitation machine," *IEEE Trans. Ind. Electron.*, vol. 64, no. 12, pp. 9943–9952, Dec. 2017.
- [11] G. Zhang, W. Hua, M. Cheng, J. Liao, K. Wang, and J. Zhang, "Investigation of an improved hybrid-excitation flux-switching brushless machine for HEV/EV applications," *IEEE Trans. Ind. Appl.*, vol. 51, no. 5, pp. 3791–3799, Sep./Oct. 2015.
- [12] Y. Wang and Z. Q. Deng, "Hybrid excitation topologies and control strategies of stator permanent magnet machines for DC power system," *IEEE Trans. Ind. Electron.*, vol. 59, no. 12, pp. 4601–4616, Dec. 2012.
- [13] C. Pollock, H. Pollock, R. Barron, J. Coles, D. Moule, A. Court, and R. Sutton, "Flux-switching motors for automotive applications," *IEEE Trans. Ind. Appl.*, vol. 42, no. 5, pp. 1177–1184, Sep./Oct. 2006.
- [14] B. C. Mecrow, T. J. Bedford, J. W. Bennett, and T. Celik, "The use of segmental rotors for 2 phase flux-switching motots," in *Proc. Int. Conf. Electr. Mach.*, Chania, Greece, 2006.
- [15] R. Qu and T. A. Lipo, "Dual-rotor, radial-flux, toroidally wound, permanent-magnet machines," *IEEE Trans. Ind. Appl.*, vol. 39, no. 6, pp. 1665–1673, Nov./Dec. 2003.



**Xing Zhao** received the B.Sc. degree from the Department of Automation at Nanjing University of Aeronautics and Astronautics, China, in 2014, and currently he is pursuing a Ph.D. degree in the department of electrical engineering at the Hong Kong Polytechnic University, Hong Kong. His research interests include the design and control of novel electric machines for the electric and hybrid electric vehicles, as well as renewable energy systems.



**Shuangxia Niu** received the B.Sc. and M.Sc. degrees in electrical engineering from the School of Electrical Engineering and Automation, Tianjin University, Tianjin, China, in 2002 and 2005, respectively, and the Ph.D. degree in electrical engineering from the Department of Electrical and Electronic Engineering, The University of Hong Kong, Hong Kong, in 2009. Since 2009, she has been with The Hong Kong Polytechnic University, Kowloon, Hong Kong, where she is currently an Assistant Professor in the Department of Electrical Engineering. She has authored or coauthored over 70 papers in leading journals. Her research interests include the design and control of novel electrical machines and drives, renewable energy conversion systems, and applied electromagnetics.



**W.N. Fu** received the B.Eng. degree in electrical engineering from Hefei University of Technology, Hefei, China, in 1982, the M.Eng. degree in electrical engineering from Shanghai University of Technology, Shanghai, China, in 1989, and the Ph.D. degree in electrical engineering from Hong Kong Polytechnic University, Hong Kong, in 1999. He is currently a Professor at Hong Kong Polytechnic University. Before joining the university in October 2007, he was one of the Key Developers at Ansoft Corporation, Pittsburgh, PA, USA. He has about seven years of working experience at Ansoft, focusing on the development of the commercial software Maxwell. He has published 184 papers in refereed journals. His current research interests mainly include numerical methods of electromagnetic field computation, optimal design of electric devices based on numerical models, applied electromagnetics, and novel electric machines and motion control.